Synthesis of Charge Transfer Complexation between 2,5-Dihydroxy-*p*-benzoquinone and 2-Amino Aniline; Spectral Characterization and DFT Analysis

L. Arunapriya[1,*,] and N. Venkatesh[2,]

[1]Department of Chemistry, Bhavan's Vivekananda College of Science, Commerce and Humanities, Sainikpuri, Secunderabad-500094, India
[2]Department of Chemistry, Osmania University, Hyderabad-500007, India

*Corresponding author: E-mail: e.arunapriya@gmail.com

A charge transfer (CT) complex was synthesized using electron donor 2-amino aniline (AA) and electron acceptor 2,5-dihydroxy benzoquinone (DHBQ) in an acetonitrile medium. The charge transfer complex stoichiometry is 1:1. The Benesi-Hildebrand equation was used to determine the molar absorptivity (ε_{CT}), association constant (K_{CT}) and other physical constants. The synthesized solid CT-complex was analyzed by ^{1}H NMR and FT-IR spectroscopic methods. DFT study of the CT complex (gas phase) at the basis set B3LYP/6-31++G also gave similar results of the experimental work. Mulliken atomic charges and reactive parameters of acceptor and donor recommend that AA is good electron donor and DHBQ is good electron acceptor so that form good highly stable charge transfer complex. Finally, good agreement between the experimental and theoretical computations was observed confirming that the basis set used is appropriate for the system under examination.

Keywords: 2-Amino aniline, 2,5-Dihydroxy-*p*-benzoquinone, Charge transfer complex, DFT study, Mulliken charges.

INTRODUCTION

An association of two or more molecules known as a charge transfer (CT) complex is one in which a portion of the electronic charge is transferred between the molecular moieties. Electron donors with a low enough ionization potential combine with electron acceptors with a high enough electron affinity to form CT-complexes [1,2]. The resultant electrostatic attraction of the fragment molecules stabilizes the molecular formation. The source molecule, from which the negative charge is trans-ferred, is referred to as electron donor and the receiving species, which is referred to as acceptor, can be conceptually separated into two halves.

In some charge transfer processes, quinone molecule forms a free radical ion from the benzoquinone radical anions created by the donor [3]. This CT-complex shows various applications like electronic, solar cell, optical devices and other applications [4,5]. Charge transfer interactions also play vital role in many biological systems [6]. In current work, the spectroscopic and theoretically analyses of the formation of solid CT-complex between 2,5-dihydroxy-*p*-benzoquinone (DHBQ), an electron

acceptor and 2-amino aniline, an electron donor, in acetonitrile as solvent using Job's continuous variation method are discussed. The synthesized solid CT complex was characterized with UV, infrared and ^{1}H NMR spectral analysis. The thermodynamic parameters of charge transfer interaction *viz.*, formation constant (K_{CT}), molecular extinction coefficient (e) and thermodynamic parameters were also calculated. To support the experimental investigation, density functional theory (DFT) method was employed utilizing the B3LYP/6-31++ (d,p) basis sets. The optimum configurations of the donor, acceptor, and charge transfer complex were computed and examined. Moreover, the geometrical characteristics were calculated, and the molecular electrostatic potential (MEP) maps were also generated to iden-tify the nucleophilic and electrophilic attacks.

EXPERIMENTAL

Preparation of standard stock solutions: A standard stock solution of 2,5-dihydroxy-*p*-benzoquinone (DHBQ, 1×10^{-2} mol L^{-1}) was prepared by dissolving 0.0351 g in 25 mL volum-etric flask using acetonitrile as solvent. A solution of donor
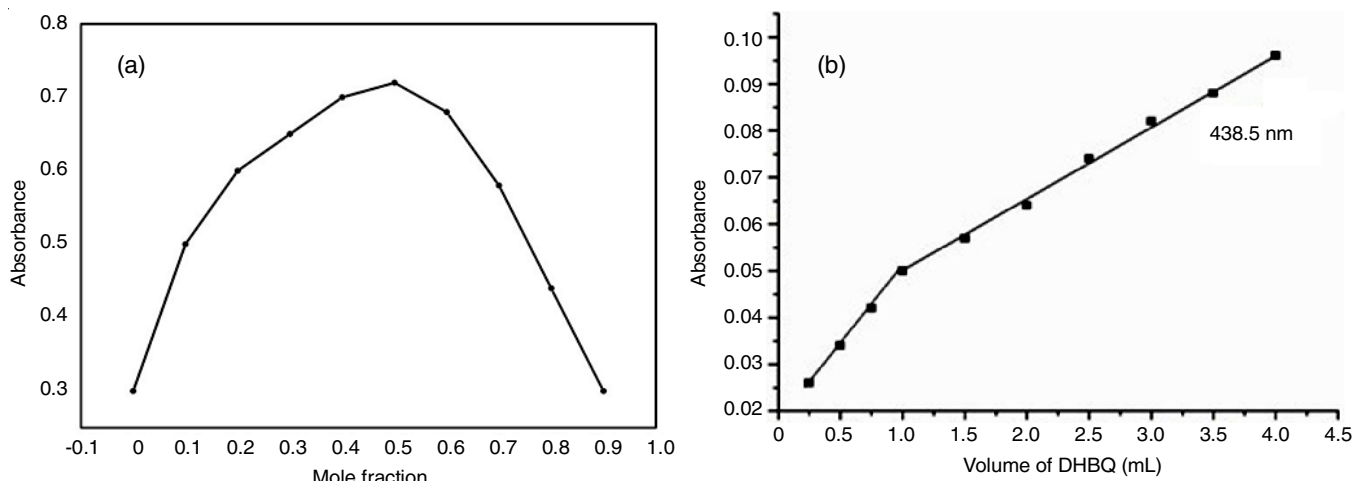
Fig. 1. Job's plot (a) and photometric titration plot (b) of CT-complex

(2-amino aniline, 1.0×10^{-3} mol L^{-1}) was prepared in different volumetric flasks by diluting 1×10^{-2} mol L^{-1} solution with the same solvent. The donor and acceptor stock solutions were preserved from exposure to light.

Preparation of solid charge transfer complex: The solid CT complex was synthesized by mixing 1:1 molar solutions of 2AA nd DHBQ in acetonitrile. The reaction mixture was continuously stirred at room temperature for 20 min, which yielded a solid CT-complex. The solid precipitate formed, was filtered, washed with acetonitrile and then dried overnight in CaCl$_2$ desiccator. Colour: violet: elemental analysis of $C_{12}H_{12}N_2O_4$; calcd. (found) %: C, 58.06 (58.10); H, 4.87 (4.81); N, 11.29 (11.28); O, 25.78 (25.80); LC-MS: *m/z* 248.08 (100.0%), 419.08 (13.9%).

Computational details: The Gaussian 09W program [7] was used for the density functional theory (DFT) calculations of the reactants and complexes in the gas phase. The geometries of the reactants (2AA, DHBQ) and CT-complexes were fully optimized at Becke three parameter Lee–Yang–Parr hybrid exchange–correlation functional (B3LYP) [8] and 6-31+G(d,p) basis set. The Gauss View 5.0.8 [9] software was used to draw the input molecular structures and also to analyze the electron density distribution in frontier molecular orbitals.

RESULTS AND DISCUSSION

Molecular composition of the CT-complex

Job's method: The Job's method of continuous variations [10] at 438.5 nm was applied to know the molecular composition of the solid CT complex. The plot of absorbance *versus* mole fraction (Fig. 1) revealed that the maximum absorbance was found at 0.5 mole fraction, which indicates the formation of a 1:1 [(2AA):(DHBQ)] CT-complex in acetonitrile.

Spectrophotometric titration method: The photometric titrations [11] were measured for the reaction of 2AA donor with DHBQ acceptor at 438.5 nm. A 0.25, 0.50, 0.75, 1.00, 1.50, 2.00, 2.50, 3.00, 3.50 and 4.00 mL aliquots of a standard solution (1.0×10^{-3} mol L^{-1}) of the appropriate acceptor in solvent were added to 1.00 mL of 2AA (1.0×10^{-3} mol L^{-1}). The total volume of the mixture was fixed to 5 mL. The concen-

tration of 2AA (C$_2$) in the reaction mixture was kept fixed at 1.0×10^{-3} mol L^{-1} while the concentration of the π-acceptor (C$_1$) changed over a wide range of concentrations from 0.25×10^{-4} mol L^{-1} to 1.0×10^{-3} mol L^{-1}, to produce solution varying ratio of donor to acceptor from 4:1 to 1:4. The stoichiometry of the molecular CT-complex was determined by the application of conventional spectrophotometric molar ratio method.

Formation constant and charge transfer energy of CT-complexes: The modified Benesi-Hildebrand equation [12] has been used to calculate the formation constant, K (L mol^{-1}) and molar extinction coefficient, ε (L mol^{-1} cm^{-1}) of the solid CT-complex.

$$\frac{C_1 \times C_2}{A} = \frac{1}{K_{CT}\varepsilon} + \frac{C_1 + C_2}{\varepsilon} \tag{1}$$

whereas C$_1$ and C$_2$ are the initial concentrations of π-acceptor (DHBQ) and donor (2AA), respectively; A is the absorbance of the CT-band. The data obtained for C$_1$ and C$_2$ then the values of (C$_1$+C$_2$) and (C$_1$× C$_2$)/A were calculated. The plot of (C$_1$× C$_2$)/A *vs.* (C$_1$+C$_2$) has been found to be a straight line with a slope of 1/ε and with an intercept of 1/K$_{CT}$ε (Fig. 2). The K and ε values for CT-complex are given in Table-1. The formation constant depends on the nature of the acceptor and donor.
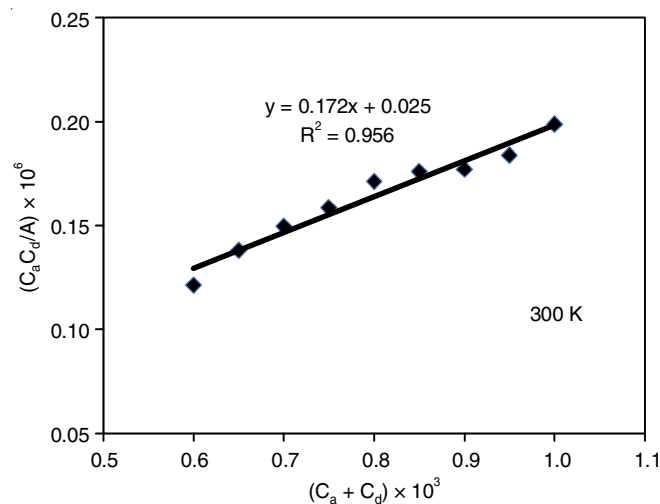

Fig. 2. The modified Benesi-Hildebrand plot of CT-complex

TABLE-1 SPECTROPHOTOMETRIC AND FREE ENERGY CHANGE RESULTS OF CT-COMPLEXES								
Complex	K_{CT} (L mol^{-1})	λ_{max} (nm)	$-\Delta G°$ (kJ mol^{-1})	E_{CT} (eV)	ε (Lmol^{-1} cm^{-1})	IP	W	R_N
CTC	6.879×10^3	438.5	-22.039	2.84	5813.95	9.24	5.03	81.11×10^2

Determination of physical parameters: The standard free energy (ΔG) for solid CT-complex was calculated using the formation constant [13], whereas the free energy change ($\Delta G°$) of complex was calculated from the following equation:

$$\Delta G° = RT \ln K_{CT} \quad (2)$$

The results of $\Delta G°$ revealed that the CT-complex formation process is spontaneous. The $\Delta G°$ values are found to be more negative as the formation constant of the solid CT-complex increases. As the bond between the components becomes stronger and thus the components are subjected to more physical strain or loss of freedom, the $\Delta G°$ value becomes more negative. The more negative value of $\Delta G°$, the longer the reaction will proceed in order to achieve equilibrium.

The energy of charge transfer (E_{CT}) for CT-complex was calculated by employing the following equation [14]:

$$E_{CT} = (h\nu_{CT}) = \frac{1243.667}{\lambda_{CT}} \quad (3)$$

where λ_{CT} is the wavelength of band (CT-complexes). The high value of K supports the anticipated high stability of the CT-complex, attributed to the electron donation from 2AA *via* the amino groups. The formation constants also depend on the nature of the acceptors.

The ionization potential (IP) of 2AA donor in the complex was calculated using the following empirical equation [15]:
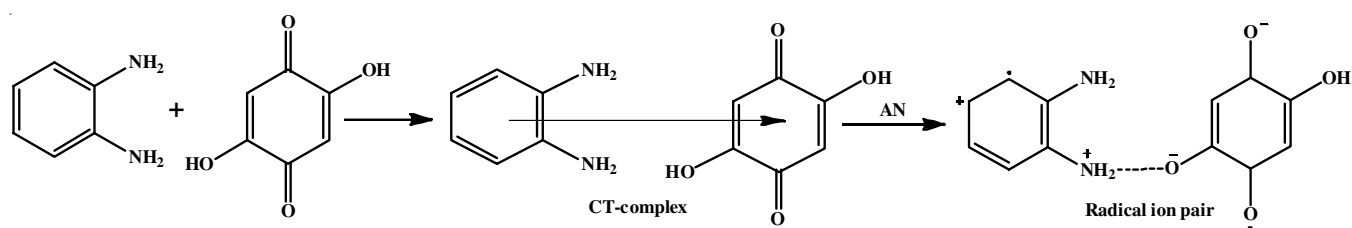
$$IP \text{ (eV)} = 5.76 + 1.53 \times 10^{-4} \nu_{CT} \quad (4)$$

where ν_{CT} is the wavenumber in cm^{-1} which corresponds to the CT band formed from the interaction between the donor and the acceptor. The electron donating power of the donor is measured in terms of its IP, the energy required to the removal of an electron from its HOMO. The dissociation energy (W) of formed solid CT-complex [16] was calculated from the corresponding CT energy (E_{CT}), the ionization potential of the donor (IP) and electron affinity (EA) of the acceptor.

$$W = IP - EA - E_{CT} \quad (5)$$

Briegleb [17] theoretically derived the following relationship to obtain the resonance energy (R_N):

$$\varepsilon_{CT} = \frac{7.7 \times 10^{-4}}{h\nu_{CT} / [R_N] - 3.5} \quad (6)$$

where ε_{CT} is the molar absorption coefficient of CT-complex at the maximum of CT absorption; ν_{CT} is the frequency of CT peak; R_N is the resonance energy of complex in the ground state, which contributes to the stability constant of the complex (a ground-state property).

Electronic spectra: The electronic absorption spectra of the charge transfer reactions of DHBQ with 2AA in acetonitrile is shown in Fig. 3. The resultant CT complex exhibits with three bands are visible between 380 and 440 nm wavelength range; the largest peak was found at 438.5 nm. The absorptions are associated with the significant colour shift observed after the reactants were combined. These alterations are a reflection of the CT complex's generated electronic transitions, which implies the formation of CT-complex and band appeared at $\lambda = 438.5$ nm for [2AA:DHBQ] complex. The existence of the CT-band shows the transfer of electrons from donor to acceptor [18]. The formation of stable violet colour is an indication of the formation of radical anion of DHBQ resulting from the electron transfer of 2AA towards DHBQ (**Scheme-I**) [19]. The acrylonitrile polymerization verified by the radical formation in the scheme [20].
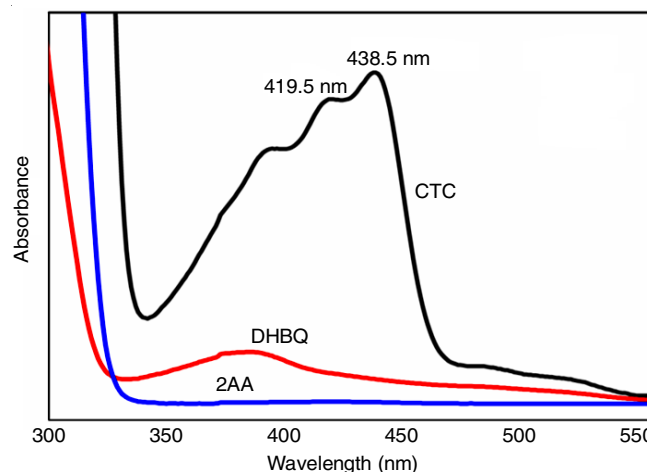

Fig. 3. Electronic spectra of 2AA, DHBQ and CT-complex

Infrared spectral studies: A broad band with a centre at 3385 cm^{-1} is found as the stretching vibration of $\nu(NH_3^+)$, which indicates the formation of a proton-transfer complex between

Scheme-I: Proton transfer mechanism between 2AA and DHBQ CT complex

2AA and DHBQ. A broad peak at 3192 cm^{-1} is due to the OH proton moved towards the nitrogen of amino group to form a proton-transfer complex between 2AA and DHBQ (Fig. 4). The infrared spectrum of the complex also shows a broad band at 1450 cm^{-1} attributing to δ(OH) overlapping with ν(C=C) of DHBQ and ν(C=N) vibrational bands of 2AA. On the other hand, ν(C=C) appears at 1633 cm^{-1} in the DHBQ spectrum whereas ν(C=N) appears at 1493 cm^{-1} in 2AA. The appearance of ν(C=O) as a weak band at 1740 cm^{-1} compared with a strong band at 1748 cm^{-1} for DHBQ. All these observations confirm the formation of a solid CT complex which suggests the proton transfer between 2AA and DHBQ.
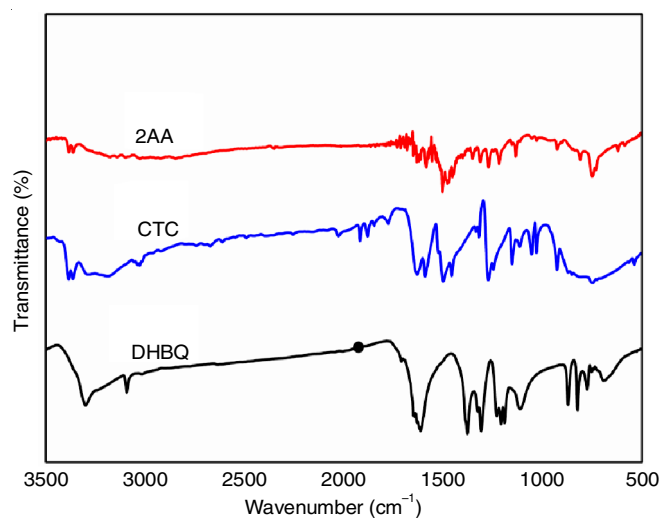

Fig. 4. FT-IR spectra of 2AA, DHBQ and CT-complex

^{1}H NMR spectral studies: The ^{1}H NMR spectrum of the solid CT-complex (2AA-DHBQ) was recorded in DMSO solvent and is shown in Fig. 5. From the ^{1}H NMR studies, the nature of interactions between the donor and acceptor in the obtained product and is shown in **Scheme-I**. The formation of the CT-complex was confirmed by the appearance of two new signals of amine group of 2AA. The protons of DMSO in the spectrum of the CT-complex appeared at δ 2.4 ppm. The amine group protons interacts with the DHBQ and another observed at the δ 5.4 ppm, which is assigned as the free amine group
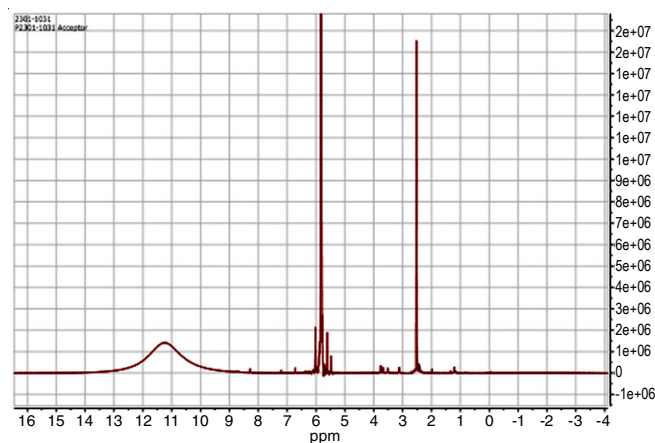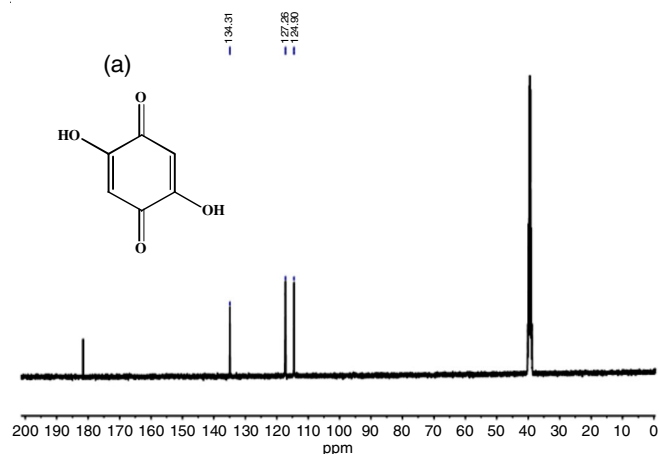

Fig. 5. ^{1}H NMR spectra of the CT-complex in DMSO

protons. The peak observed at δ 6.0-7.0 ppm in the CT-complex is due to the aromatic nature of 2AA. The O-H peak of DHBQ observed at δ 11 ppm as a broad signal. The proton signals of the 2AA (donor) in CT-complex has shifted downfield or higher ppm values indicates transfer of π-electrons from donor to acceptor.

^{13}C NMR spectral studies: The charge transfer interactions in the studied solid CT-complex are further evident using ^{13}C NMR spectrum of CT-complex is shown in Fig. 6. The chemical shifts of carbon atom (C=O) in DHBQ is δ 182 ppm, this value has reduced in the solid CT-complex. From these observations, the carbon atom signals of DHBQ in the CT-complex confirmed its formation. It can be also observed the upfield shift of the carbon atom signals of DHBQ (lower chemical shift) due to the increase of electron density from the charge transfer from 2AA (donor).

Computational DFT studies: The computational density functional theory analysis was carried out according to Becke's three parameter Lee–Yang–Parr Gradient-corrected correlation potential (B3LYP) and important calculations were performed by using 6-31++G basis set. This model has been widely used for geometry optimization and the determination of electronic properties. The optimized values of bond lengths, bond angles, molecular electrostatic potential map values, characterization of the frontier molecular orbital [21] surfaces and Mulliken
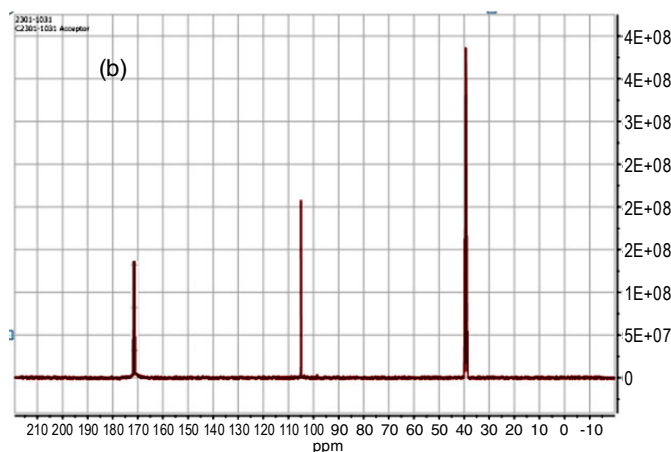

Fig. 6. ^{13}C NMR spectra of (a) DHBQ and (b) CT-complex in DMSO

atomic charges were produced. The optimized geometries of 2AA, DHBQ and 1:1 CT complex with atomic number are shown in Fig. 7.

The optimized geometrical bond length values are compiled in Table-2, which shows that the carbon oxygen bond length of DHBQ in CTC C5–O13 and C2–O14 of the DHBQ moieties of the CT-complex increased to 1.2639 and 1.2782 Å compared with 1.2593 Å and 1.2593 Å for free DHBQ. This result suggests that the carbon–oxygen bond length in DHBQ is greater than that of the double bond in free DHBQ, verifying the electron transfer from the donor ring and nitrogen to the carbon–oxygen bond of DHBQ. It is worth to mention that the orientation of the 2AA electron moiety was found to be oriented towards the DHBQ and this orientation producing the resona-ting structure from the electron transfer to DHBQ of the solid CT-complex. This indicates the π-electron transfer from the HOMO of 2AA to the π*LUMO of carbonyl groups of DHBQ moiety. The C2-N14, C3-N11 bond lengths decreased to 1.3924 Å, 1.3853 Å compared with 1.4071 Å and 1.4070 Å, respectively of free 2AA, which clearly indicate that ring carbon electron density involving in solid CT-complex formation. It indicates the electron density on donor moiety of the complex decreases, which results in the contraction of bond lengths compared to donor alone.

The solid CT-complex is further confirmed from the changes in its bond angles as compared to the reactants as shown in Table-3. The bond angles of C1-C2-N14 and C4-C3-N11 of 2AA/CTC were also decreased (122.32º to 120.76º and 122.32º to 120.88º) indicating the strain relief of CT-complex. The free radical anion of DHBQ was also supported from the change in bond angles of C1-C2-O14 and C4-C5-O13 of CTC (116.49º to 115.61º and 116.49º to 116.21º). In case of 2AA, the bond angles between ring carbon atoms decreases in the solid CT-complex as compared to 2AA alone, which confirms the π–π* transition from HOMO to LUMO molecular orbitals of the characterized solid CT-complex.

Molecular electrostatic potential surfaces: The MEP quantifies the attractiveness or repulsiveness of a molecular area to a proton positioned at any location in the surrounding area [22]. The MEP surfaces were calculated by the DFT method

Parameter	DHBQ bond length (Å)	2AA bond length (Å)	CT complex bond length (Å)
C(1)-C(2)	1.5115		1.4993
C(1)-C(6)	1.357		1.3598
C(2)-C(3)	1.442		1.4300
C(6)-C(5)	1.442		1.4383
C(3)-C(4)	1.357		1.3631
C(5)-C(4)	1.5115		1.5054
C(5)-O(13)	1.2593		1.2639
C(2)-O(14)	1.2593		1.2782
C(1)-O(9)	1.355		1.3568
C(4)-O(11)	1.355		1.3516
C(1)-C(2)		1.4024	1.4054
C(1)-C(6)		1.4018	1.3961
C(2)-C(3)		1.4192	1.4292
C(6)-C(5)		1.4000	1.4015
C(5)-C(4)		1.4018	1.3953
C(3)-C(4)		1.4023	1.4080
C(2)-N(14)		1.4071	1.3924
C(3)-N(11)		1.4070	1.3853

TABLE-2
GROUND STATE (DFT) GEOMETRIC BOND LENGTH
VALUES (Å) OF 2AA, DHBQ AND CT COMPLEX

(B3LYP) and basis set (6-31++G) used for geometry optimization, as shown in Fig. 8. The acceptor (DHBQ) MEP plot is characterized by a positive region (blue) is located at the centre (0.0299 a.u.), the negative charge region comes from O (-0.0376 and -0.0262 a.u.) of DHBQ. The donor (2AA) major negative region (red) is located on the ring C and N atoms (-0.0370 and -0.0327 a.u.). The donor (2AA) interacts with acceptor (DHBQ) positive region of acceptor (DHBQ) consequently; the value decreased to 0.0207 a.u. and the donor (2AA) electron density on ring C' atom is decreased to -0.0268 a.u. These results confirmed the electron transfer from π-electrons of the ring atoms of 2AA to C=O groups of DHBQ.

Frontier molecular orbital (FMO) energies calculation for CT complex: Molecular orbital analysis shows that the frontier molecular orbitals are mainly composed of *p*-orbitals [23]. HOMO-LUMO calculation of 2AA ~ DHBQ complex in ground state obtained by DFT method with basis set (6-31 ++G) at B3LYP is shown in Fig. 9. It is clear that LUMOs are mainly delocalized on the DHBQ moiety; while HOMOs are
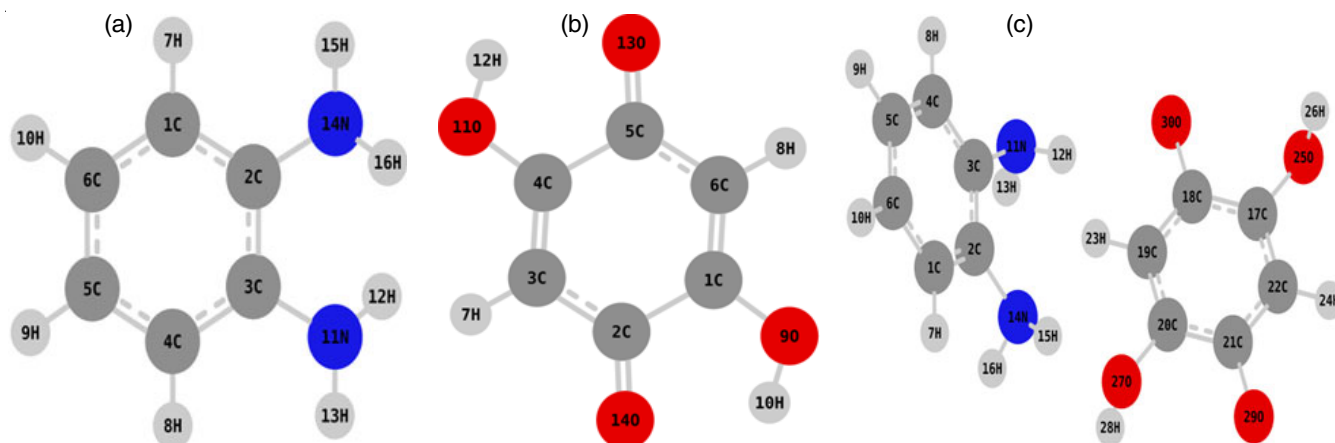

Fig. 7. DFT optimized geometries of the complex in gas phase (a) 2AA (b) DHBQ (c) 2AA~DHBQ CT complex

TABLE-3
OPTIMIZED BOND ANGLES OF 2AA, DHBQ AND CTC

| Parameter	DHBQ	DHBQ/CTC	Parameter	2AA	2AA/CTC
C(1)-C(2)-C(3)	118.69	119.22	C(2)-C(1)-C(6)	120.89	121.45
C(2)-C(1)-C(6)	122.51	122.45	C(1)-C(2)-C(3)	119.31	119.01
C(1)-C(6)-C(5)	118.79	118.82	C(2)-C(3)-C(4)	119.31	118.60
C(4)-C(5)-C(6)	118.69	118.35	C(3)-C(4)-C(5)	120.89	121.52
C(3)-C(4)-C(5)	122.51	122.78	C(4)-C(5)-C(6)	119.77	119.78
C(2)-C(3)-C(4)	118.79	118.37	C(1)-C(6)-C(5)	119.77	119.63
C(4)-C(5)-O(13)	116.49	116.21	C(1)-C(2) -N(14)	122.32	120.76
C(6)-C(5)-O(13)	124.81	125.44	C(3)-C(2) -N(14)	118.36	120.22
C(3)-C(2)-O(14)	124.81	125.16	C(4)-C(3) -N(11)	122.32	120.88
C(1)-C(2)-O(14)	116.49	115.61	C(2)-C(3) -N(11)	118.36	120.50
C(3)-C(4)-O(11)	122.67	123.04			
C(5)-C(4)-O(11)	114.82	114.17			
C(2)-C(1)-O(9)	114.82	114.60			
C(6)-C(1)-O(9)	122.67	122.94			
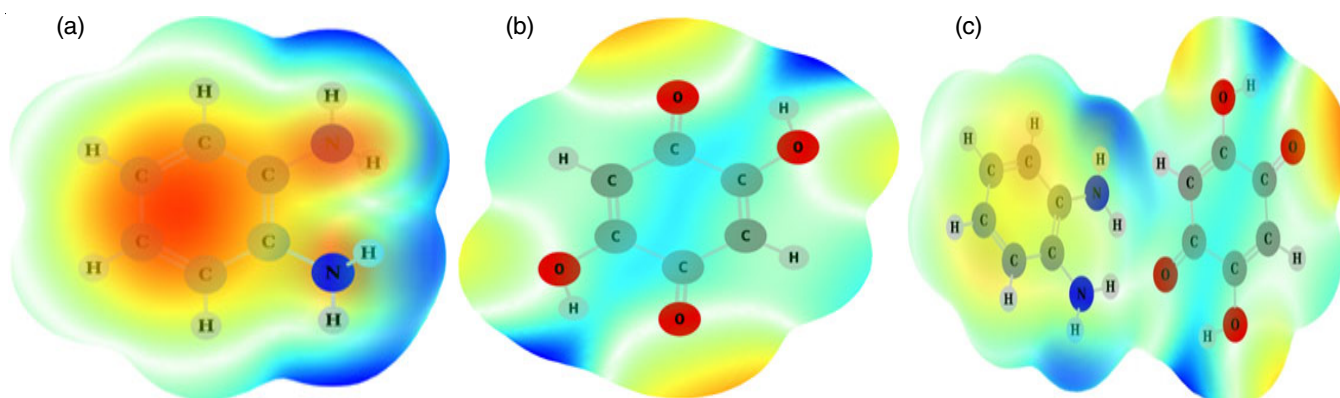
Fig. 8. Molecular electrostatic potential (MEP) maps for (a) 2AA (b) DHBQ and (c) 2AA~DHBQ CT complex in ground state calculated using DFT calculation
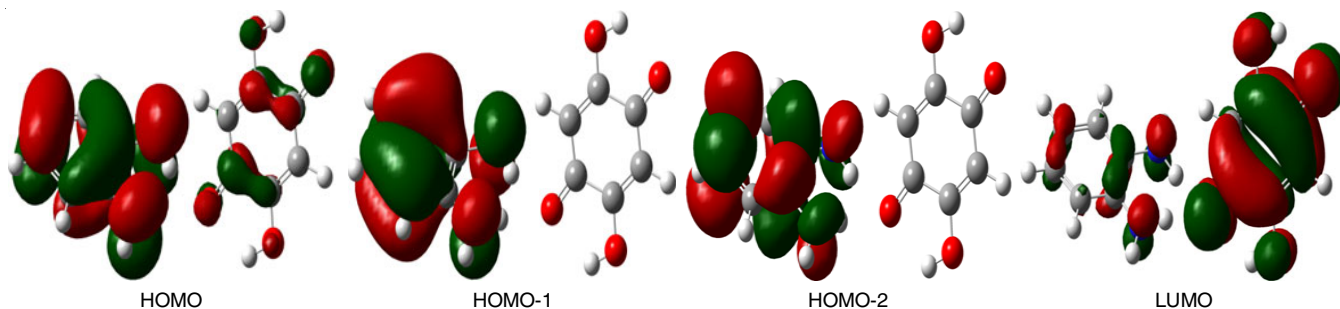

Fig. 9. Important molecular orbital pictures of 2AA~DHBQ complex calculated by DFT (6-31++G)

localized on 2AA only. The molecular orbital HOMO's are localized on 2AA part of the complex and hence, one concludes that the π-electrons are localized in HOMO's molecular orbital, this HOMO can be considered as π-molecular orbitals and LUMO is π* molecular orbital. Consequently, the observed transitions can be assigned to be π−π* transitions.

The energy values for HOMO and LUMO of 2AA, DHBQ and 2AA~DHBQ complex in ground state are provided in hatrees (Table-4). It is observed that LUMO energy level of 2AA~DHBQ CT complex (-0.14671 Ha) compares well with the LUMO energy level of DHBQ (-0.1578 Ha), while HOMO energy (-0.17108 Ha) level of the CT- complex are close to HOMO energy level of 2AA (-0.1895 Ha). This reason for the localization of frontier molecular orbital's of 2AA~DHBQ complex system

TABLE-4
HOMO-LUMO ENERGY VALUES FOR DHBQ,
2AA AND CT COMPLEX IN OPTIMIZED STATE

Molecular orbital	Orbital energy (Hatree)		
	DHBQ	2AA	2AA~DHBQ complex 6-31++G
HOMO	-0.2812	-0.1895	-0.17108
HOMO-1	-0.3056	-0.2252	-0.21497
HOMO-2	-0.3122	-0.3012	-0.26442
HOMO-3	-0.3214	-0.3104	-0.29031
HOMO-4	-0.3978	-0.3504	-0.29508
LUMO	-0.1578	-0.0154	-0.14671
LUMO+1	-0.0352	-0.0006	-0.01489
LUMO+2	-0.0222	0.0014	-0.00648
LUMO+3	-0.0175	0.0043	0.02083
LUMO+4	-0.0052	0.0176	0.03470

is too similar to other electron donor–acceptor composites. Hence, the orbital interaction energy arises mainly due to the charge transfer between occupied and unoccupied orbitals.

Reactivity descriptors from computational studies: The reactivity parameters such as ionization potential (I), electron affinity (A), chemical potential (μ), hardness (η) and electrophilicity index (ω), softness (σ) all derived from the HOMO and LUMO energies, have been proposed for understanding various aspects of reactivity with chemical reactions [24]. The following equations provided for these parameters.

$$I = -E_{HOMO} \tag{7}$$

$$A = -E_{LUMO} \tag{8}$$

$$\eta = \frac{I - A}{2} \tag{9}$$

$$\mu = -\frac{I + A}{2} \tag{10}$$

$$\omega = \frac{\mu^2}{2\eta} \tag{11}$$

$$\sigma = \frac{1}{\eta} \tag{12}$$

The electronic parameters of DHBQ and 2AA molecules is shown in Table-5. From the HOMO and LUMO energies, molecules with higher E_{HOMO} values are superior electron donors. In contrast, those having lower E_{LUMO} values are superior electron acceptors. From this point of view, DHBQ is discriminated by lower E_{LUMO} value than 2AA. On the other hand, 2AA has a higher E_{HOMO} than the DHBQ and it is thus considered the electron donor in the reaction. Moreover, the chemical potential is a parameter that indicates the direction of electron transfer among the molecules. Electron flow occurs from system with a higher μ value to the one with a lower μ value. From this point of view, 2AA has a higher μ value than DHBQ. The electrophilicity index (ω) measures the electron philicity of molecule. Since DHBQ has high ω value, the former molecule is better electrophile than the latter one. The values of 'σ' and all these results revealed that 2AA is an electron donor, whereas DHBQ is an electron acceptor.

TABLE-5 ELECTRONIC REACTIVITY DESCRIPTORS OF THE DHBQ AND 2AA		
Parameter	DHBQ gas phase	2AA gas phase
E_{HOMO} (eV)	-7.6518	-5.1565
E_{LUMO} (eV)	-4.2939	-0.4190
I	7.6518	5.1565
A	4.2939	0.4190
η	1.6789	2.3687
μ	-5.9728	-2.7877
ω	10.6243	1.6404
σ	0.5956	0.4221

CONFLICT OF INTEREST

The authors declare that there is no conflict of interests regarding the publication of this article.

REFERENCES

1. J.-Y. Zhang, L.-L. Wang and X.-Q. Zhu, *ACS Phys. Chem Au*, **3**, 358 (2023);
https://doi.org/10.1021/acsphyschemau.3c00001
2. G.E. Milanovsky, A.A. Petrova, D.A. Cherepanov and A.Y. Semenov, *Photosynth. Res.*, **133**, 185 (2017);
https://doi.org/10.1007/s11120-017-0366-y
3. C. Balraj, A. Satheshkumar, K. Ganesh and K.P. Elango, *Spectrochim. Acta A: Mol. Biomol. Spectrosc.*, **114**, 256 (2013);
https://doi.org/10.1016/j.saa.2013.05.031
4. S.H. Oh, B.G. Kim, S.J. Yun, M. Maheswara, K. Kim and J.Y. Do, *Dyes Pigments*, **85**, 37 (2010);
https://doi.org/10.1016/j.dyepig.2009.10.001
5. J.E. Benedetti, A.D. Gonçalves, A.L.B. Formiga, M.-A. De Paoli, X. Li, J.R. Durrant and A.F. Nogueira, *J. Power Sources*, **195**, 1246 (2010);
https://doi.org/10.1016/j.jpowsour.2009.09.008
6. M.H. Barary, M.H. Abdel-Hay, S.M. Sabry and S.T. Belal, *J. Pharm. Biomed. Anal.*, **34**, 221 (2004);
https://doi.org/10.1016/j.japna.2003.08.007
7. A. Becke, *J. Chem. Phys.*, **98**, 5648 (1993);
https://doi.org/10.1063/1.464913
8. L. Arunapriya, V. Srimai, N. Venkatesh, K. Jaeyoung, J. Joonkyung and T. Parthasarathy, *J. Biomol. Struct. Dyn.*, **42**, 2793 (2023);
https://doi.org/10.1080/07391102.2023.2212785
9. R.D. Dennington, T.A. Keith and J.M. Millam, GaussView 5.0.8, Gaussian (2008).
10. H.M. Elqudaby, G.G. Mohamed and G.M.G. El-Din, *Spectrochim. Acta A Mol. Biomol. Spectrosc.*, **129**, 84 (2014);
https://doi.org/10.1016/j.saa.2014.02.110
11. D.A. Skooge, Principle of Instrumental Analysis, Sunder College Publisher, New York, edn. 3 (1985).
12. H.A. Benesi and J.H. Hildebrand, *J. Am. Chem. Soc.*, **71**, 2703 (1949);
https://doi.org/10.1021/ja01176a030
13. W.B. Person, *J. Am. Chem. Soc.*, **84**, 536 (1962);
https://doi.org/10.1021/ja00863a007
14. A.A. Ibrahim, *Afr. J. Pure Appl. Chem*, **5**, 507 (2011).
15. A.M.A. Adam, M. Salman, T. Sharshar and M.S. Refat, *Int. J. Electrochem. Sci.*, **8**, 1274 (2013);
https://doi.org/10.1016/S1452-3981(23)14097-1
16. H. McConnell, J.S. Ham and J.R. Platt, *J. Chem. Phys.*, **21**, 66 (1953);
https://doi.org/10.1063/1.1698626
17. G. Briegleb, Elektronen-Donator-Acceptor-Komplexe, Springer-Verlog, Berlin (1961).
18. K.M. Al-Ahmary, M.M. Habeeb and E.A. Al-Solmy, *J. Solution Chem.*, **39**, 1264 (2010);
https://doi.org/10.1007/s10953-010-9591-0
19. G.A. Saleh, H.F. Askal, M.F. Radwan and M.A. Omar, *Talanta*, **54**, 1205 (2001);
https://doi.org/10.1016/S0039-9140(01)00409-X
20. T. Parthasarathy, K. Nageshwar Rao, B. Sethuram and T.N. Rao, *J. Macromol. Sci Chem. A.*, **23**, 955 (1986);
https://doi.org/10.1080/00222338608081103
21. A. Lakkadi, N. Baindla, S. Vuppala and P. Tigulla, *J. Phys. Org. Chem.*, **30**, e3700 (2017);
https://doi.org/10.1002/poc.3700
22. A. Lakkadi, N. Baindla and P. Tigulla, *J. Solution Chem.*, **46**, 2171 (2017);
https://doi.org/10.1007/s10953-017-0685-9
23. K.M. Al-Ahmary, S.M. Soliman, R.A. Mekheimer, M.M. Habeeb and M.S. Alenezi, *J. Mol. Liq.*, **231**, 602 (2017);
https://doi.org/10.1016/j.molliq.2017.02.038
24. V. Choudhary, A. Bhatt, D. Dash and N. Sharma, *J. Comput. Chem.*, **40**, 2354 (2019);
https://doi.org/10.1002/jcc.26012